Journal of Molecular Structure 1278 (2023) 134835

Contents lists available at ScienceDirect

Journal of Molecular Structure

journal homepage: www.elsevier.com/locate/molstr

Investigation of substituent effect on rhenium complexes by DFT methods: Structural analysis, IR spectrum, quantum chemical parameter, NLO and OLED properties, molecular docking

Ceylan Alkaya Yıldız*, Elif Güney, Vesim Nasif, Duran Karakaş, Sultan Erkan

Chemistry Department, Faculty of Science, Cumhuriyet University, Sivas 58140, Turkey

ARTICLE INFO

Article history:
Received 26 July 2022
Revised 16 December 2022
Accepted 19 December 2022
Available online 5 January 2023

Keywords:
Rhenium complexes
DFT calculations
Optic properties
Molecular docking

ABSTRACT

For the synthesized 9b, 9c and 9d complexes, hypothetical complexes were formed by adding electron-withdrawing (NO_2) and electron-donating (NH_2) groups. Benchmark analysis was performed using the bond lengths of the synthesized complexes (9b, 9c and 9d). B3LYP-LANL2DZ/6-31+G(d), B3LYP-LANL2DZ/6-31G(d), B3LYP-SDD/6-31+G(d), B3LYP-SDD/6-31G(d), M062X-LANL2DZ/6-31+G(d), M062X-LANL2DZ/6-31G(d), M062X-SDD/6-31+G(d) and M062X-SDD/6-31G(d) levels were used for these analysis. According to the correlation coefficient, the best level was determined as M062X-SDD/6-31+G(d). IR spectra of all complexes were examined in detail. Experimental results and calculation results for IR spectra were found to be in agreement with each other. The activities of the complexes were compared with the quantum chemical parameters. It was predicted that complexes containing electron donor groups are more advantageous in terms of biological activity. Electrophilic and nucleophilic regions for complexes were determined by molecular orbitals diagrams and electrostatic potentials maps. In addition, all complexes were evaluated in terms of their optical properties (NLO and OLED) and were found suitable for both materials. Experimentally, the 9b, 9c and 9d complexes were active against the A2780 ovarian cancer cell lines. Therefore, molecular docking was performed with the selected protein (PDB ID: 5FI4) and all complexes. The obtained computational results were found to be in agreement with the experimental data.

1. Introduction

Recently, it has been reported that a significant number of organometallic compounds are strongly toxic to cancer cells, and organometallic compounds are used in newly investigated anticancer drug candidates [1]. Rhenium complexes have an important place in photodynamic therapy and photoactive chemotherapy, thanks to their broad spectroscopic and photophysical properties [2]. The outer shell of Re(I) contains six electrons in the electron configuration. Form low spin octahedral complexes. Thanks to this configuration, Re(I) tricarbonyl complexes are kinetically inert and therefore devoid of toxicity compared to other heavy metals [3]. It forms new complexes of homonuclear $Re(CO)_3$ with pyridine-containing ligands, which can have profound effects on its biological properties [4]. In the [Re(I)(N^N)(CO)3L] complex, the neutral bidentate diimine ligand (N^N) is the moiety that regulates its optoelectric properties, and X is a halogen or electron rich group. Re(I) complexes are recommended for use as emissive emitters in OLEDs due to their easy synthesis, short phosphorescent life and outstanding luminescence properties [5]. The excited states of [Re(I)(N^N)(CO)3L] complexes cause metal-ligand charge transfer (MLCT). With this transition, it makes complex luminescence. Thus, its excited states have the most suitable photophysical properties for biological imaging [6]. In addition, Re(I) tricarbonyl complexes have the ability to be precisely detected in cells [7].

In this study, nine rhenium complexes were discussed. 9b, 9c and 9d complexes were synthesized and hypothetical complexes were formed by adding electron-withdrawing (NO_2) and electron-donating (NH_2) groups for these synthesized complexes and the effect of the groups was investigated. The complexes were evaluated structurally by detailed analysis of bond lengths, bond angles and IR spectra. Biological activities of complexes, highest energy occupied molecular orbital energy (E_{HOMO}), lowest unoccupied molecular orbital energy (E_{LUMO}), the difference between HOMO and LUMO energy (ΔE), hardness (η), softness (σ), electronegativity (χ), chemical potential (μ), global molecular electrophilicity (ω) index, global molecular nucleophilicity (ε) index, electron-accepting (ω^+) and electron-donating (ω^-) index.

* Corresponding author.
E-mail address: ceylanalkaya21@gmail.com (C.A. Yıldız).

https://doi.org/10.1016/j.molstruc.2022.134835
0022-2860/

Table 1
The calculated bond lengths (Å) by using the B3LYP, experimental bond lengths (Å) and correlation coefficients (R2) for 9b, 9c and 9d complexes.

			Re−N1	Re−N2	Re−Cl1	Re−C1	Re−C2	Re−C3	R^2
LANL2DZ	6-31+G(d)	**9b**	2.186	2.203	2.553	1.912	1.929	1.922	0.9798
		9c	2.186	2.203	2.549	1.914	1.929	1.922	0.9978
		9d	2.185	2.203	2.550	1.914	1.929	1.922	0.9945
	6-31G(d)	**9b**	2.211	2.226	2.520	1.920	1.931	1.924	0.9931
		9c	2.211	2.226	2.517	1.922	1.931	1.925	0.9982
		9d	2.210	2.226	2.517	1.922	1.931	1.925	0.9989
SDD	6-31+G(d)	**9b**	2.201	2.216	2.552	1.924	1.942	1.935	0.9827
		9c	2.201	2.216	2.548	1.926	1.943	1.936	0.9989
		9d	2.200	2.217	2.548	1.926	1.943	1.936	0.9960
	6-31G(d)	**9b**	2.221	2.234	2.517	1.932	1.945	1.939	0.9931
		9c	2.221	2.234	2.514	1.934	1.945	1.939	0.9979
		9d	2.221	2.234	2.514	1.934	1.945	1.939	0.9983
		Exp.	2.171	2.215	2.422	1.9421	1.931	1.916	

Frontier molecular orbitals and molecular electrostatic potential (MEP) maps were interpreted. In addition, all complexes were evaluated for their optical properties (NLO and OLED). The computationally investigated rhenium complexes, ovarian cancer was evaluated by molecular insertion studies with the target protein PDB ID = 5FI4 corresponding to the A2780 cell line.

2. Calculations techniques

Three-dimensional structures of the complexes were plotted in Gauss-View 6.0.0 [8] and calculated in Gaussian 09 AML64L-Revision C.01 [9]. Calculations for each complex were performed using DFT-B3LYP [10] and M062X [11] methods and LANL2DZ/6-31+G(d), LANL2DZ/6-31G(d), SDD/6-31+G(d) and SDD/6-31G(d) basis sets [12].

3. Result and discussion

3.1. Benchmark analysis and optimized structures

Comparing sets of benchmark errors is an important tool for evaluating theories in computational chemistry [13]. The idea behind the benchmark concept is to measure the relative behavior of chemicals rather than the absolute value of a particular behavioral trait [14]. Benchmark analysis is the most important step in computational chemistry [15]. Computational chemistry offers multiple levels of computation for the studied chemical species. The correlation between an experimental parameter and the calculated parameter is given by the correlation coefficient (R^2) values. Closer to 1 and/or 1 for "R^2" increases the accuracy of the calculation level. Experimental bond lengths of the 9b, 9c and 9d complexes synthesized by Wilson et al. were compared with the calculated bond lengths by using DFT-B3LYP and M062X methods and LANL2DZ-6-31+G(d), LANL2DZ-6-31G(d), SDD-6-31+G(d) and SDD-6-31G(d) basis sets. The calculated bond lengths by using the B3LYP and M062X methods are listed in Tables 1 and 2, respectively.

According to the R^2 values obtained by considering the bond lengths in Tables 1 and 2, the greatest closeness between the experimental and calculated bond lengths for the three complexes was obtained at the M062X-SDD/6-31+G(d) level. For this purpose, all calculations after this section for both the synthesized and hypothetical complexes were performed at the M062X-SDD/6-31+G(d) level. The optimized structures of the 9b, 9c, 9d, 9b-NH_2, 9c-NH_2, 9d-NH_2 and 9b-NO_2, 9c-NO_2, 9d-NO_2 complexes with the M062X-SDD/6-31+G(d) level are shown in Table 1.

3.2. Vibrational spectrum

In computational chemistry, each of the fundamental vibrational motions results from the atoms changing their bond lengths and bond angles, and these vibrational motions correspond to a vibrational frequency. Vibrational spectra containing vibration frequencies give important information about molecular structure [16]. The IR spectra of all rhenium complexes were calculated at M062X/SDD/6-31+G(d,p) level. Calculated IR spectra are given in Fig. 2 with peak numbers.

3.2.1. C–H vibrational analysis

In general, the CH bond stretching frequencies of the complexes were observed in the range of 3200–3050 cm^{-1}. The first region in the spectra was labeled as the C–H bond stretching region. It was observed that aromatic C–H bond stretching frequencies were higher than aliphatic bond stretching frequencies. However, the molar absorption coefficients of the aromatic C–H

Table 2
The calculated bond lengths (Å) by using the M062X, experimental bond lengths (Å) and correlation coefficients (R2) for 9b, 9c and 9d complexes.

			$Re-N_1$	$Re-N_2$	$Re-Cl_1$	$Re-C_1$	$Re-C_2$	$Re-C_3$	R^2
LANL2DZ	6-31+G(d)	**9b**	2.198	2.209	2.550	1.898	1.919	1.912	0.9852
		9c	2.200	2.210	2.546	1.899	1.919	1.912	0.9997
		9d	2.199	2.210	2.547	1.899	1.919	1.912	0.9970
	6-31G(d)	**9b**	2.232	2.239	2.521	1.907	1.920	1.915	0.9939
		9c	2.233	2.240	2.517	1.909	1.920	1.915	0.9933
		9d	2.232	2.240	2.517	1.909	1.920	1.915	0.9951
SDD	**6-31+G(d)**	**9b**	2.214	2.223	2.551	1.907	1.928	1.921	**0.9878**
		9c	2.215	2.224	2.547	1.908	1.928	1.922	**0.9996**
		9d	2.215	2.224	2.548	1.908	1.928	1.922	**0.9975**
	6-31G(d)	**9b**	2.244	2.248	2.520	1.916	1.930	1.925	0.9934
		9c	2.246	2.250	2.516	1.918	1.930	1.925	0.9909
		9d	2.245	2.250	2.518	1.918	1.930	1.925	0.9930
		Exp.	2.171	2.215	2.422	1.9421	1.931	1.916	

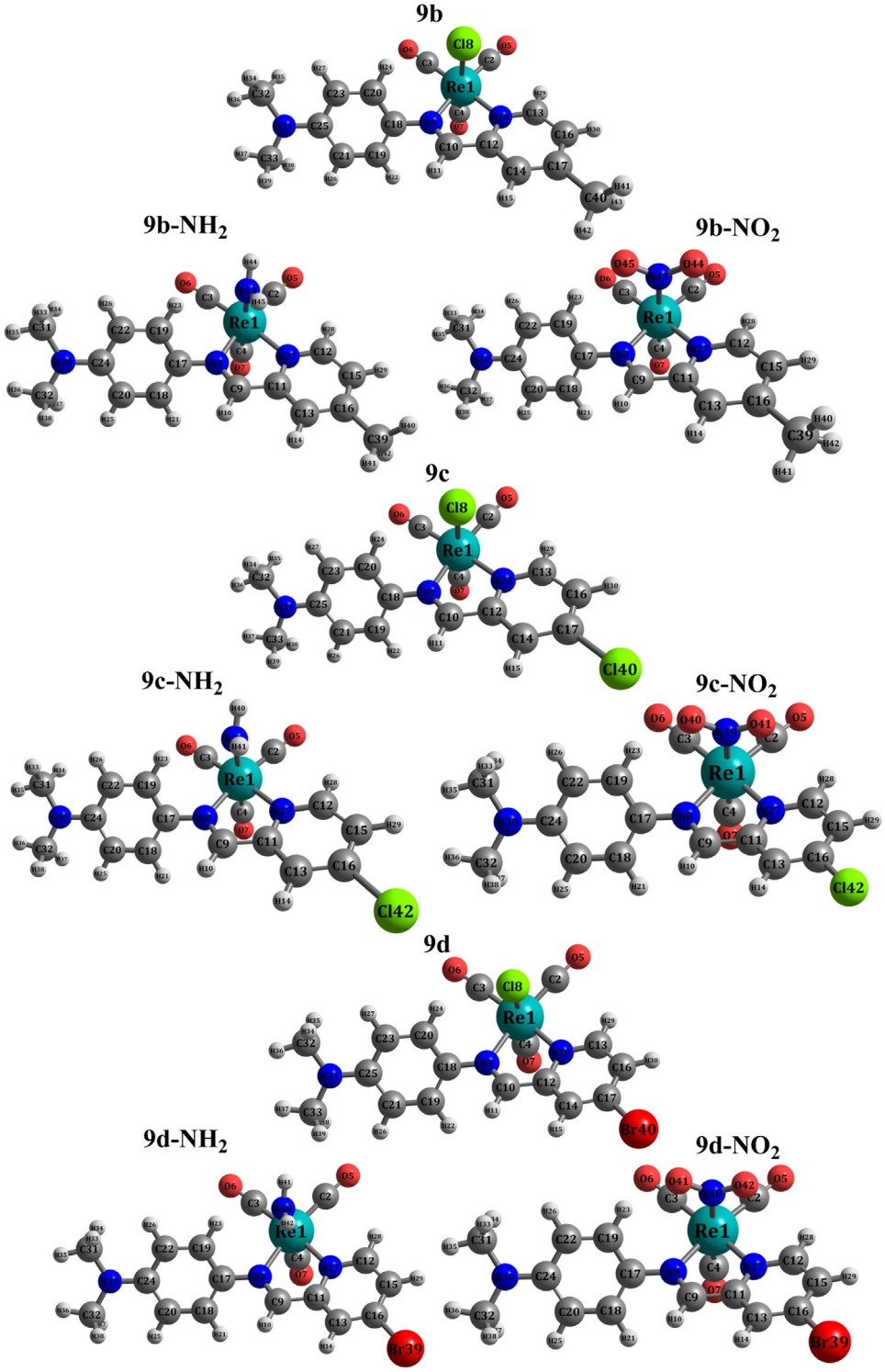

Fig. 1. Calculated optimized structures of the studied rhenium complexes at the M062X-SDD/6-31+G(d) level.

bond strain modes were found to be lower. C–H bond stretch frequencies for the 9b complex were calculated as 3201.74, 3112.94 and 3048.64 cm^{-1}. C–H bond stresses were observed at 3198.07, 3108.11 and 3046.56 cm^{-1} for the 9b-NH_2 complex. The C–H bond regression frequencies for the 9b-NO_2 molecule are 3199.94, 3111.89 and 3048.06 cm^{-1}. Similarly, the 9c and 9d complexes and their NH_2 and NO_2 forms have nearly close C–H bond strain frequencies. These values show that the change in the electron withdrawing and donor properties of the ligand attached to the central atom does not cause a change in the C–H bond stresses of the substituent containing the aliphatic moiety.

3.2.2. C–O bond stretching

Experimentally synthesized 9b, 9c and 9d complexes have carbonyl bond stretch frequencies. The CO bond stretching frequency for the 9b complex is experimentally 2016, 1907 and 1880 cm^{-1}. Carbonyl bond strectch frequencies of 2055.13, 1965.70 and 1940.48 cm^{-1} were calculated for the M062X/SDD/6-31+G(d,p)

level. Although the calculated frequencies were harmonic frequencies, the results were found to be quite consistent with the experimental values. CO bond stretching for 9b-NH_2 are 2030.61, 1934.54, 1914.78 cm^{-1}, for 9b-NO_2 the CO bond stretching are 2060.73, 1970.55, 1958.59 cm^{-1} in gas phase with the level M062X/SDD/6-31+G(d,p) calculated. This caused an increase in the CO bond stretching frequencies of the NH_2 structure. It can be said that this situation increases the back-bonding of the carbonyl ligand compared to the NO_2 ligand of NH_2. This is indicative of the electron donor property of the NH_2 ligand. This situation is also observed in 9c-NH_2, 9c-NO_2, 9d-NH_2 and 9d-NO_2 complexes. The experimental CO bond stretching for the 9c and 9d complex are 2018, 1930, 1856 and 2017, 1923, 1848 cm^{-1}, respectively. These results were obtained with the calculation level as 2056.98, 1969.17, 1944.19 and 2056.76, 1968.87, 1943.91 cm^{-1}. Experimental and calculation results were found to be compatible with each other. As with the 9b complex, the CO bond stretch frequencies are higher in the 9c and 9d complexes containing the NO_2 ligand (2032.54, 1938.14, 1918.59 and 2032.31, 1937.89, 1918.39 cm^{-1}, 9c-NO_2 and 9d-NO_2 for 9c-NH_2 and 9d-NH_2, respectively). for 2062.74, 1974.11, 1962.13 and 2062.55, 1973.94, 1961.89 cm^{-1}, respectively)

3.2.3. N–H bond stretching

Experimentally, there is no N–H bond stretching frequency. N–H bond stretching frequencies at the level of M062X/SDD/6-31+G(d,p) are 3648.44 cm^{-1} and 3521.75 $cm^{-1}$for the 9b-NH_2 complex; It was calculated as 3531.08 cm^{-1} for the 9c-NH_2 complex and 3528.54 cm^{-1} for the 9d-NH_2 complex. N–H bond stretching frequency values are theoretically 3500 cm^{-1}. Frequency values calculated at M062X/SDD/6-31+G(d,p) level are in the range of 3500–3650 cm^{-1}.

3.2.4. C–C bond stretching

Experimentally, there is no aromatic C–C bond stretch frequency. Caro-Caro bond stretch frequencies at the M062X/SDD/6-31+G(d,p) level are 1700 cm^{-1}, 1637.85 cm^{-1} and 1645.73 cm^{-1} for the 9b complex; 1699.04 cm^{-1}, 1644.18 cm^{-1} and 1634.65 cm^{-1} for the 9b-NH_2 complex; 1700.46, 1643.76 and 1637.27 cm^{-1} for the 9b-NO_2 complex one; 1681.60, 1677.26, 1643.54 and 1635.95 cm^{-1} for the 9c complex; 1674.21 cm^{-1}, 1642.28 cm^{-1} and 1632 for the 9c-NH_2 complex; 1679.88 cm^{-1}, 1673.27 cm^{-1}, 1641.22 cm^{-1} and 1634.33 cm^{-1} for the 9c-NO_2 complex; 1716.41 cm^{-1}, 1675.63 cm^{-1}, 1645.08 cm^{-1} and 1632.67 cm^{-1} for the 9d complex; 1677.41 cm^{-1}, 1673.58 cm^{-1}, 1643.36 cm^{-1}, 1629.21 cm^{-1} for the 9d-NH_2 complex; It was calculated as 1679.68 cm^{-1}, 1671.86 cm^{-1}, 1642.80 cm^{-1} and 1631.70 cm^{-1} for the 9d-NO_2 complex.

Theoretically, Caro-Caro bond stretching frequency values are in the range of 1670–1600 cm^{-1} and the frequency values calculated at M062X/SDD/6-31+G(d,p) level are in the range of 1700–1500 cm^{-1}. According to the results, the Caro-Caro bond stretching frequency values are consistent with the theoretical results.

3.2.5. C–N bond stretching

Experimentally, there is no C=N bond stretching frequency. C=N bond stretching frequencies at the level of M062X/SDD/6–31+G(d,p) 1684.57, 1637.85, 1601.77 cm^{-1} for the 9b complex, 1682.72, 1634.65, 1600.79 cm^{-1}, 9b for the 9b-NH_2 complex 9b-NO_2 complex 1678.45, 1637.27, 1602.04 cm^{-1}, for 9c complex 1681.60, 1677.26, 1635.95, 1602.80 cm^{-1}, for 9c-NH_2 complex 1632.55, 1602.02 cm^{-1}, for 9c-NO_2 complex 1673.27, 1634.33, 1603.14 cm^{-1} for the 9d complex 1716.41, 1675.63, 1632.67, 1602.96 cm^{-1} for the 9d-NH_2 complex 1677.41, 1629.21, 1601.82 cm^{-1} for the 9d-NO_2 complex 1679.68, 1671.86, 1631.70, It was calculated as 1603.08 cm^{-1}. In the IR Spectra for the complexes in Fig. 2, these regions are labeled as C=N bond stretching regions.

C=N frequency values are theoretically in the range of 1690–1640 cm^{-1}. C=N bond stretching frequency values calculated at M062X/SDD/6-31+G(d,p) level are in the range of 1700–1600 cm^{-1} and are theoretically compatible.

3.2.6. Bending region

The bending zone is known as bending vibrations in bonds as opposed to bond stretching [17]. Generally, bond angles vary in this region. Wagging, scissoring, rocking and twisting may occur in the bending region, depending on the type of angle change. In the Infrared Spectra in Fig. 2, the bending zone was determined for each complex. For all the complexes studied, this range is generally 1250–600 cm^{-1}.

3.2.7. Re-C bond stretching

The bond stretching frequency between the central atom and the groups attached to it is 652.61 cm^{-1} and 480.77 cm^{-1} for the 9b complex with the help of animation; 658.50 cm^{-1} and 484.89 cm^{-1} for the 9b-NH_2 complex; 653.19 cm^{-1} and 479.57 cm^{-1} for the 9b-NO_2 complex; 652.03 cm^{-1} and 481.36 cm^{-1} for complex 9c; 657.99 cm^{-1} and 484.51 cm^{-1} for the 9c-NH_2 complex; 652, cm^{-1} and 458.91 cm^{-1} for the 9c-NO_2 complex; 651.72 cm^{-1} and 480.53 cm^{-1} for the 9d complex; 657.91 cm^{-1} and 484.57 cm^{-1} for the 9d-NH_2 complex; It is 652.30 cm^{-1} and 478.89 cm^{-1} for the 9d-NO_2 complex.

3.2.8. Re-Cl bond stretching

Re-Cl bond stretchings were observed for the 9b, 9c and 9d complexes with the help of bond stretching frequency animation between the central atom and the groups attached to it. Re-Cl bond stretching frequencies of these complexes were found as 274.16, 275.02, and 274.19 cm^{-1}, respectively (Fig. 2).

3.3. Quantum chemical parameters

The frontier molecular orbitals are the highest energy occupied molecular orbital (HOMO) and the lowest energy non-bonding vacant molecular orbital (LUMO) energies. The increase in the energy of the HOMO can be associated with the decrease in the energy of the LUMO, respectively, with the electron donating and uptake capacity of the chemical species [18]. The difference (ΔE) between HOMO and LUMO energy allows predictions about molecular stability and reactivity [19]. Due to the nature of the maximum stiffness principle, hard molecules have a high energy gap (ΔE) value. Due to electronic construction principles, hardness is a measure of stability. Softness is the opposite of hardness. In terms of biological activity, chemical species should have low hardness and high softness. Electronegativity can be characterized as the electron attraction capacity, almost similarly to the electrophilicity index. Chemical potential and nucleophilicity index are related to this electron donating capacity. Decreased values of electronegativity and electrophilicity index and increasing values of chemical potential and nucleophilicity index are considered advantageous for activity prediction. The last parameter is electron donation power and electron acceptance power parameters are also related to electron exchange [20]. Quantum chemical parameters are calculated as follow:

$$I = -E_{HOMO} \quad (1)$$

$$A = -E_{LUMO} \quad (2)$$

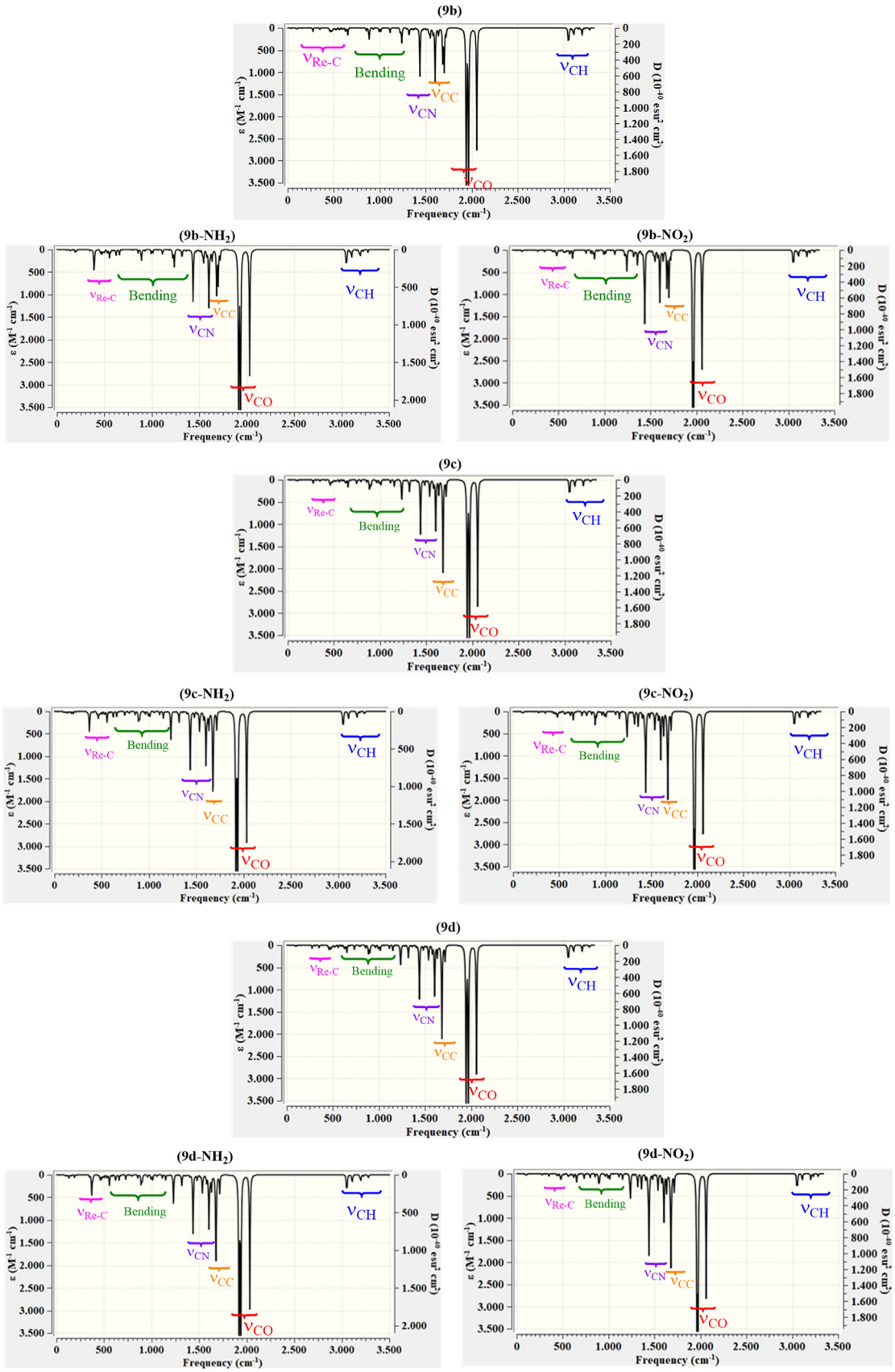

Fig. 2. Calculated IR spectra of studied rhenium complexes.

Table 3
Quantum chemical parameters of investigated rhenium complexes.

	9b	9b-NH_2	9b-NO_2	9c	9c-NH_2	9c-NO_2	9d	9d-NH_2	9d-NO_2
E_{HOMO}*	−6.6916	−5.4791	−6.7139	−6.8464	−5.6355	−6.8709	−6.8274	−5.6246	−6.8519
E_{LUMO}*	−1.9938	−1.7834	−2.1228	−2.3239	−2.1143	−2.4490	−2.2912	−2.0844	−2.4164
ΔE*	4.6978	3.6956	4.5911	4.5226	3.5212	4.4219	4.5362	3.5402	4.4355
η^*	2.3489	1.8478	2.2956	2.2613	1.7606	2.2109	2.2681	1.7701	2.2177
σ^{**}	0.4257	0.5412	0.4356	0.4422	0.5680	0.4523	0.4409	0.5649	0.4509
χ^*	4.3427	3.6313	4.4183	4.5852	3.8749	4.6600	4.5593	3.8545	4.6341
μ^{**}	−4.3427	−3.6313	−4.4183	−4.5852	−3.8749	−4.6600	−4.5593	−3.8545	−4.6341
Ω	4.0144	3.5680	4.2521	4.6486	4.2642	4.9109	4.5826	4.1967	4.8417
ε	0.2491	0.2803	0.2352	0.2151	0.2345	0.2036	0.2182	0.2383	0.2065
Ω^+	2.0578	1.3378	1.5932	1.7430	1.5913	1.8388	1.7184	1.5677	1.8137
w-	6.479	5.615	6.748	7.224	6.422	7.517	7.146	6.345	7.436
A	296.6867	299.4385	299.9781	301.328	304.361	305.186	305.871	308.996	309.682

*eV, **; eV^{-1}.

$$\mu = -\chi = \left[\frac{\partial E}{\partial N}\right]_{v(r)} = -\left(\frac{I+A}{2}\right) \quad (3)$$

$$\eta = \frac{1}{2}\left[\frac{\partial^2 E}{\partial N^2}\right]_{v(r)} = \frac{I-A}{2} \quad (4)$$

$$\sigma = 1/\eta \quad (5)$$

$$\omega = \chi^2/2\eta = \mu^2/2\eta \quad (6)$$

$$\varepsilon = 1/\omega \quad (7)$$

$$\omega^+ = (I+3A)^2/(16(I-A)) \quad (8)$$

$$\omega^- = (3I+A)^2/(16(I-A)) \quad (9)$$

In line with generalizations, the order of biological activity according to the increase in E_{HOMO}, softness, chemical potential and nucleophilicity index and electron donating and accepting power, and decrease in E_{LUMO}, ΔE, hardness, electronegativity, and electrophilicity index is as follows:

9d>9c>9b

9b-NH_2>9b>9b-NO_2

9c-NH_2>9c>9c-NO_2

9d-NH_2>9d>9d-NO_2

3.4. Molecular orbitals and electrostatic potentials

Contour diagrams of frontier molecular orbitals, on the other hand, can provide useful information in determining the atomic surfaces that play an active role during electron acquisition and transfer [21]. Molecular electrostatic potential (MEP) is widely used to obtain information about molecular size, shape and electrostatic potential values. Molecular modeling is a useful method for studies such as reactive parts in chemical reactions and naming biological processes. The values of the electrostatic potentials of the surface are defined with different colors. yellow, red, orange, green and blue, and the color order of the potentials is red < orange < yellow < green < blue. The yellow and red color on the MEP surface is the negatively charged and electron-rich region. The region indicated in blue is positively charged and represents the electron-poor region. The region indicated in green is a neutral region that does not express potential [22]. Contour diagrams of the frontier molecular orbitals of the complexes and molecular electrostatic potential maps are given in Figs. 3 and 4, respectively.

According to the Contour diagrams, the HOMO and LUMO molecular orbital electron densities are on the pi conjugated systems. If the complexes give or receive Electrons, this also means that they absorb a light, indicating that they will correspond to $\pi \rightarrow \pi^*$ transitions. The central atom electron density does not play an efficient path in HOMO→LUMO transitions. There is an electronic transition from N,N-Dimethyl-p-phenylenediamine to picolinaldehyde unit. It can be thought that π delocalization is important in electronic transitions, and it will increase the NLO and OLED properties of the complexes.

The red and yellow regions are the negative and electron rich regions. According to Fig. 4, the region of N,O and Re in 9b-NO_2, 9c-NO_2, 9d-NO_2 structures is the electron-dense region. In 9b, 9c, 9d structures, the electron-rich region is in 9b; It is seen that there is an electron density originating from the O atom in the 9b-NH_2, 9c-NH_2, 9d-NH_2 structures. The fact that the blue region is more in 9b, 9b-NH_2, and 9b-NO_2 compared to the other structures on the MEP surface indicates that the mentioned regions are electron-poor. It is observed that there is no electrostatic potential in the molecules except 9b, 9b-NH_2, and 9b-NO_2, especially in the regions where Cl and Br atoms are located, and there is a neutral region.

3.5. NLO properties

Metal coordination compounds with nonlinear optical (NLO) properties have been investigated for modern communication technology products in recent years. A systematic study of the electronic structure and nonlinear properties of metal complexes is of great importance in this regard. DFT studies developed with computational chemistry techniques can reveal the NLO properties of complexes [23].

Total static dipole moment (μ), mean linear polarizability (α), polarizability anisotropy ($\Delta\alpha$) and first hyperpolarizability (β) [24] of complexes including standard urea were used to predict NLO properties, and these numerical values are given in Table 4.

$$\mu = \left(\mu_x^2 + \mu_y^2 + \mu_z^2\right)^{1/2} \quad (10)$$

$$a = \frac{1}{3}(a_{xx} + a_{yy} + a_{zz}) \quad (11)$$

$$\Delta a = \frac{1}{\sqrt{2}}\left[(a_{xx}-a_{yy})^2 + (a_{yy}-a_{zz})^2 + (a_{zz}-a_{xx})^2 + 6a_{xz}^2 + 6a_{xy}^2 + 6a_{yz}^2\right]^{1/2} \quad (12)$$

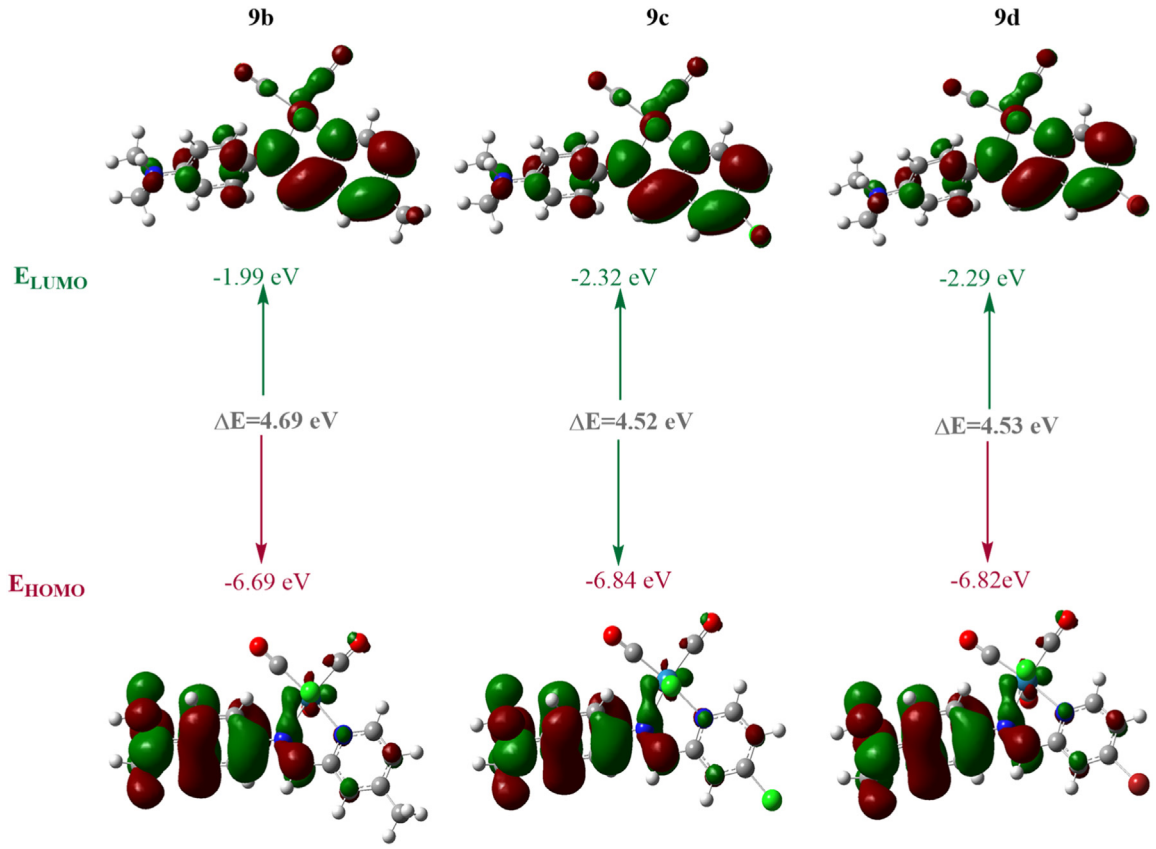

Fig. 3. Frontier molecular orbitals of studied complexes.

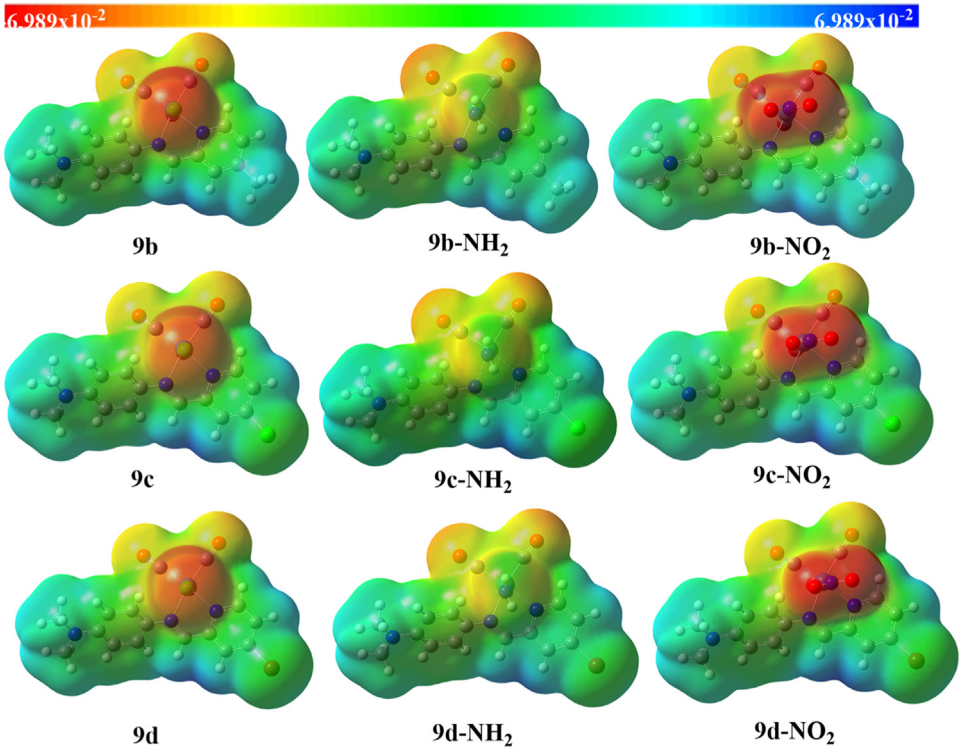

Fig. 4. MEP maps of investigated rhenium complexes.

Table 4
The calculated total static dipole moment(μ), the average linear polarizability (α), the anisotropy of the polarizability ($\Delta\alpha$), first hyperpolarizability (β).

Parameters	μ[a]	α[b]	$\Delta\alpha$[b]	β[c]
Urea	1.6523	4.6250	7.9523	$4.25x10^{-26}$
9b	6.2562	10.5541	70.3601	$1.94x10^{-25}$
9b-NH_2	6.3265	11.2653	71.0130	$1.88x10^{-25}$
9b-NO_2	6.3865	11.3542	71.3654	$2.80x10^{-25}$
9c	5.9809	10.9512	69.9684	$2.55x10^{-25}$
9c-NH_2	5.8025	10.0120	70.0148	$2.77x10^{-25}$
9c-NO_2	6.5942	10.4215	69.5239	$2.85x10^{-25}$
9d	5.1563	9.5123	66.2635	$4.86x10^{-26}$
9d-NH_2	5.1230	9.2101	66.0014	$4.08x10^{-26}$
9d-NO_2	5.2603	9.7123	66.8963	$4.91x10^{-26}$

[a]In Debye, [b]In Å^3, [c]In cm^5/esu, [d]In eV

Table 5
The reorganization energies, adiabatic/vertical ionization potentials and electron affinities (all in eV) of (2)–(6) and (2′)–(6′).

	$\lambda_{e\ (eV)}$	$\lambda_{h\ (eV)}$	IPa	IPv	EAa	EAv
9b	0.203	0.245	2.012	1.123	0.586	0.664
9b-NH_2	0.185	0.213	2.325	1.101	0.456	0.615
9b-NO_2	0.208	0.279	2.325	1.231	0.591	0.677
9c	0.203	0.253	2.624	1.254	0.557	0.726
9c-NH_2	0.199	0.234	2.785	1.109	0.453	0.706
9c-NO_2	0.235	0.280	2.331	1.345	0.488	0.758
9d	0.244	0.236	1.968	1.485	0.622	0.934
9d-NH_2	0.201	0.224	2.007	1.401	0.614	0.925
9d-NO_2	0.265	0.285	1.986	1.436	0.714	0.969

$$\beta = \left[\left(\beta_{xxx} + \beta_{xyy} + \beta_{xzz}\right)^2 + \left(\beta_{yyy} + \beta_{yzz} + \beta_{yxx}\right)^2 + \left(\beta_{zzz} + \beta_{zxx} + \beta_{zyy}\right)^2\right]^{1/2} \quad (13)$$

The total static dipole moment(μ), mean linear polarization (α), polarization anisotropy ($\Delta\alpha$) and first hyperpolarization (β) values given in Table 4 are the basic parameters for estimating the NLO properties. According to the obtained data, the investigated complexes are superior in terms of all parameters producing standard substances. Increasing values of total static dipole moment(μ), mean linear polarization (α), polarization anisotropy ($\Delta\alpha$) and first hyperpolarization (β) parameters provide superiority in terms of NLO significance. According to the results listed in Table 4, it was predicted that it could be evaluated as a good NLO material compared to reference materials urea.

3.6. Light emitting properties

An important factor in predicting the performance of OLEDs is the reorganization energy (λ) [25]. The electron transport layer (ETL) and a hole transport layer (HTL) between the cathode and an anode, the electron injection layer adjacent to the cathode (EIL) and the hole injection layer adjacent to the anode (HIL) parameters can be calculated for charge mobility of the OLED material [26]. The electron transport layer (ETL), a hole transport layer (HTL) between the cathode and an anode, and in addition to these layers, the electron injection layer adjacent to the cathode (EIL) and the hole injection layer adjacent to the anode (HIL) parameters were calculated and were given Table 5.

$$\lambda_e = \left(E_0^- - E_-^-\right) + \left(E_-^0 - E_0^0\right) \quad (14)$$

$$\lambda_h = \left(E_0^+ - E_+^+\right) + \left(E_+^0 - E_0^0\right) \quad (15)$$

Where E_0^+ and E_0^- are the energies of the cation and anion of neutral molecule. E_+^+ and E_-^- are the energies of the cation and anion obtained from cation and anion. E_+^0 and E_-^0 are the energy of the neutral molecule calculated at the cationic and anionic state. E_0^0 is the energy of the neutral molecule at the ground state.

Another parameter are adiabatic/vertical ionization potentials (IPa/IPv) and adiabatic/vertical electron affinities (EAa/EAv) [27]. These parameters are obtained from Eqs. (16)–(19).

$$IPa = E_+^+ - E_0^0 \quad (16)$$

$$IPv = E_0^+ - E_0^0 \quad (17)$$

$$EAa = E_0^0 - E_-^- \quad (18)$$

$$EAv = E_0^0 - E_0^- \quad (19)$$

Here E_0^- and E_0^+ are the energy of the re-optimized anion (cation). E_-^- (E_+^+)is the energy of the anion (cation) calculated with the optimized anion (cation) structure, E_-^0 (E_+^0) is the energy of the neutral molecule calculated at the anionic (cationic) state. In addition, E_0^0 is defined as the energy of the neutral molecule at the ground state [22].

The reference material for ETL compounds is tris(8-hydroxyquinoline) aluminum complex (Alq3) [28], while the reference material for HTL compounds is N,N'-diphenyl-N,N'-.bis(3-methylphenyl)-1,1′-diphenyl-4,4′-diamine (TPD) [29]. A good OLED material should have parameters superior to reference materials.

To get an idea of the charge transfers characteristics, it is necessary to evaluate the capabilities of λe, λh, IP, and EA, respectively. Lower reorganization energy values will encourage a higher skip rate. When the OLED parameters for the complexes are examined, it can be said that NH_2 substituents are more advantageous than other groups. On the contrary, NO_2 groups cause a disadvantage. The ionization potential (IP) and electron affinity (EA) can be used to evaluate the hole and electron injection energy barriers of OLED materials. Materials with smaller IP act as good hole carriers, while materials with larger EA are compatible with electron transport devices. While there is a trend between the IP values for the complex, this is the opposite for the EA values. For complexes with these approaches, it can be said that it is more advantageous than Alq3 as ETL materials. For the HTL material, the λh values of all the complexes are less than the λh value of the TPD.

3.7. Molecular docking

The molecular Docking method has an important place in many chemistry and cancer studies. As can be seen recently in literature, it has become a necessity in computational studies. It is an effective approach to understanding the receptor binding affinities of complexes and ligand-receptor interaction. The binding energies between the protein to be determined according to the cancer type and the chemical species investigated can be determined. In this way, the activities of chemical species on biological macromolecules can be discussed [30] Docking calculations were performed with HEX 8.0.0 [31]. The target protein representing the A2780 ovarian cancer cell line was selected as PDB ID = 5FI4 [32] for the investigated rhenium complexes. The binding energies between the studied rhenium complexes and the target protein are given in Table 6 and the interaction poses are in Fig. 5.

Anti-cancer activity is associated with the binding energy. A negative increase in binding energy increases biological activity. When the binding energies of the complexes are examined in Table 6, the anticancer activity of the complexes containing the NH_2 substituent is higher than the other complexes. The binding

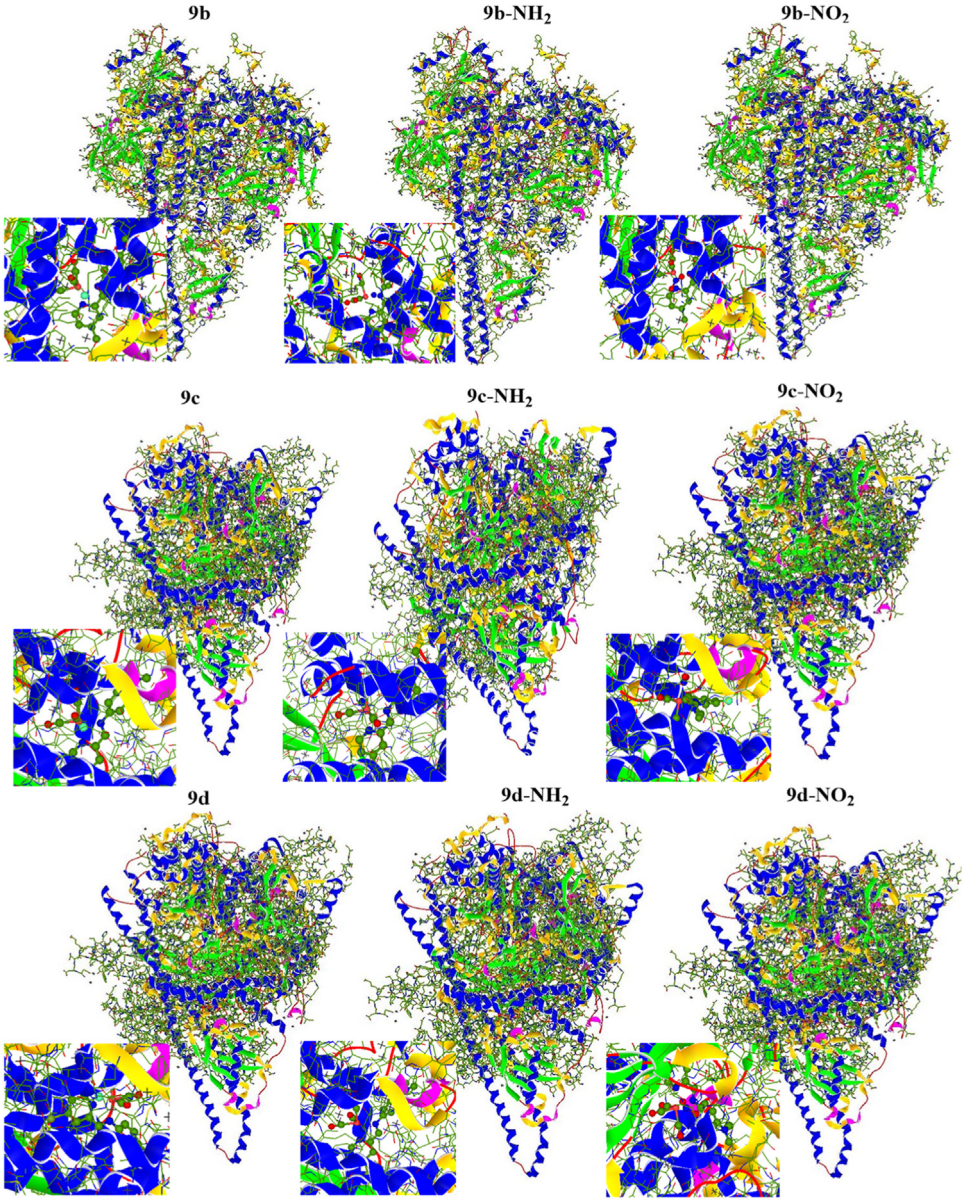

Fig. 5. The interaction poses between the rhenium complexes and target protein.

Table 6
Binding energies between investigated rhenium complexes and 5FI4 target protein.

Complexes	Binding Energies (kcal/mol)
9b	−320.18
9b-NH_2	−320.32
9b-NO_2	−319.11
9c	−318.98
9c-NH_2	−320.13
9c-NO_2	−309.98
9d	−329.23
9d-NH_2	−347.61
9d-NO_2	−316.62
Cis-Pt	−127.13

energies of 9b-NO_2, 9c-NO_2 and 9d-NO_2 complexes with NO_2 substituents are generally lower than the others. The binding energies of the 9c, 9c-NH_2 and 9c-NH_2 complexes are −318.98, −320.13 and −339.98 kcal/mol, respectively. This is in good agreement with the activity sequence obtained by quantum chemical parameters. In addition, rhenium complexes interact with the target protein at different sites.

4. Conclusion

Rhenium tricarbonyl complexes were analyzed by computational chemistry methods. The structural parameters of the existing complexes (9b, 9c and 9d) were found to be compatible with the experimental results. Structural parameters were predicted for the hypothetical complexes (9b-NH_2, 9b-NO_2, 9c-NH_2, 9c-NO_2, 9d-NH_2, 9d-NO_2). The IR spectra of all studied complexes were analyzed in detail. The activities of the complexes were predicted by quantum chemical parameters. The activity order of the synthesized complexes is 9d>9c>9b. This sorting is in agreement with the IC50 values against the experimental A2780 cell line. In addition, complexes containing NH_2 substituent are more active than complexes containing NO_2 substituents. The parameters for the NLO and OLED properties of the studied complexes were calculated. It was predicted that it could be evaluated as a good NLO and OLED material compared to reference materials. All complexes

were docked on the 5FI4 target protein representing the A2780 cell line. The substituent effect is similar to quantum chemical parameters.

Declaration of Competing Interest

The authors declare that they have no known competing financial interests or personal relationships that could have appeared to influence the work reported in this paper.

CRediT authorship contribution statement

Ceylan Alkaya Yıldız: Writing – review & editing, Methodology, Investigation. **Elif Güney:** Methodology. **Vesim Nasif:** Visualization. **Duran Karakaş:** Investigation, Formal analysis. **Sultan Erkan:** Writing – review & editing.

Data Availability

Data will be made available on request.

References

[1] A. Leonidova, V. Pierroz, R. Rubbiani, Y. Lan, A.G. Schmitz, A. Kaech, G. Gasser, Photo-induced uncaging of a specific *Re* (I) organometallic complex in living cells, Chem. Sci. 5 (10) (2014) 4044–4056.

[2] AJ. Lees, Photophysics of Organometallics, 29, Springer Science & Business Media, 2010.

[3] A.J. Amoroso, M.P. Coogan, J.E. Dunne, V. Fernández-Moreira, J.B. Hess, A.J. Hayes, C. Williams, Rhenium fac tricarbonyl bisimine complexes: biologically useful fluorochromes for cell imaging applications, Chem. Commun. (29) (2007) 3066–3068.

[4] Z. Huang, J.J. Wilson, Therapeutic and diagnostic applications of multimetallic rhenium (I) tricarbonyl complexes, Eur. J. Inorg. Chem. 2021 (14) (2021) 1312–1324.

[5] G.W. Zhao, J.H. Zhao, Y.X. Hu, D.Y. Zhang, X. Li, Recent advances of neutral rhenium (I) tricarbonyl complexes for application in organic light-emitting diodes, Synth. Met. 212 (2016) 131–141.

[6] B.L. Murphy, S.C. Marker, V.J. Lambert, J.J. Woods, S.N. MacMillan, J.J. Wilson, Synthesis, characterization, and biological properties of rhenium (I) tricarbonyl complexes bearing nitrogen-donor ligands, J. Organomet. Chem. 907 (2020) 121064.

[7] H.C. Bertrand, S. Clède, R. Guillot, F. Lambert, C. Policar, Luminescence modulations of rhenium tricarbonyl complexes induced by structural variations, Inorg. Chem. 53 (12) (2014) 6204–6223.

[8] R.D. Dennington, T.A. Keith, C.M. Millam, (2009). GaussView 5.0 Wallingford. In *CT*.

[9] M.E. Frisch, G.W. Trucks, H.B. Schlegel, G.E. Scuseria, M.A. Robb, J.R. Cheeseman, D.J. Fox. (2016). Gaussian 16.

[10] J. Paier, M. Marsman, G. Kresse, Why does the B3LYP hybrid functional fail for metals? J. Chem. Phys. 127 (2) (2007) 024103.

[11] M. Walker, A.J. Harvey, A. Sen, C.E. Dessent, Performance of M06, M06-2X, and M06-HF density functionals for conformationally flexible anionic clusters: M06 functionals perform better than B3LYP for a model system with dispersion and ionic hydrogen-bonding interactions, J. Phys. Chem. A 117 (47) (2013) 12590–12600.

[12] S. Chiodo, N. Russo, E. Sicilia, LANL2DZ basis sets recontracted in the framework of density functional theory, J. Chem. Phys. 125 (10) (2006) 104107.

[13] M.P. Waller, H. Braun, N. Hojdis, M. Bühl, Geometries of second-row transition-metal complexes from density-functional theory, J. Chem. Theory Comput. 3 (6) (2007) 2234–2242.

[14] V.A. Rassolov, M.A. Ratner, J.A. Pople, P.C. Redfern, L.A. Curtiss, 6-31G* basis set for third-row atoms, J. Comput. Chem. 22 (9) (2001) 976–984.

[15] P. Pernot, A. Savin, Probabilistic performance estimators for computational chemistry methods: systematic improvement probability and ranking probability matrix. I. Theory, J. Chem. Phys. 152 (16) (2020) 164108.

[16] M.S. McLachlan, H. Zou, T. Gouin, (2017). Using benchmarking to strengthen the assessment of persistence. Environ. Sci. Technol. 2017, 51, 4–11.

[17] K. Sayin, D. Karakaş, S.E. Kariper, T.A. Sayin, Computational study of some fluoroquinolones: structural, spectral and docking investigations, J. Mol. Struct. 1156 (2018) 172–181.

[18] S. Erkan, S. Kaya, K. Sayin, D. Karakaş, Structural, spectral characterization and molecular docking analyses of mer-ruthenium (II) complexes containing the bidentate chelating ligands, Spectrochim. Acta Part A 224 (2020) 117399.

[19] J.P. Devlin, J. Sadlej, V. Buch, Infrared spectra of large H2O clusters: new understanding of the elusive bending mode of ice, J. Phys. Chem. A 105 (6) (2001) 974–983.

[20] Y. Wu, W. Zhu, Organic sensitizers from D–π–A to D–A–π–A: effect of the internal electron-withdrawing units on molecular absorption, energy levels and photovoltaic performances, Chem. Soc. Rev. 42 (5) (2013) 2039–2058.

[21] M. Bendikov, F. Wudl, D.F. Perepichka, Tetrathiafulvalenes, oligoacenenes, and their buckminsterfullerene derivatives: the brick and mortar of organic electronics, Chem. Rev. 104 (11) (2004) 4891–4946.

[22] R. Çakmak, E. Başaran, S. Kaya, S. Erkan, Synthesis, spectral characterization, chemical reactivity and anticancer behaviors of some novel hydrazone derivatives: experimental and theoretical insights, J. Mol. Struct. 1253 (2022) 132224.

[23] A. El Aatiaoui, M. Koudad, T. Chelfi, S. Erkan, M. Azzouzi, A. Aouniti, A. Oussaid, Experimental and theoretical study of new Schiff bases based on imidazo (1, 2-a) pyridine as corrosion inhibitor of mild steel in 1 M HCl, J. Mol. Struct. 1226 (2021) 129372.

[24] H.H. Khalid, S. Erkan, N. Bulut, Halogens effect on spectroscopy, anticancer and molecular docking studies for platinum complexes, Optik 244 (2021) 166324 (Stuttg).

[25] S.A. Gungor, I. Sahin, O. Gungor, S.E. Kariper, F. Tumer, M. Kose, Pamoic acid esters and their xanthene derivatives: flourimetric detection of nitroaromatic compounds and non-linear optical properties, Sens. Actuators B 255 (2018) 3344–3354.

[26] S. Erkan, D. Karakaş, Computational investigation of structural, nonlinear optical and anti-tumor properties of dinuclear metal carbonyls bridged by pyridyl ligands with alkyne unit, J. Mol. Struct. 1199 (2020) 127054.

[27] H. Kırpık, S. Erkan, M. Kose, A new 3-substituted BODIPY dye: synthesis, crystal structure, photophysical, non-linear optic and OLED properties, J. Mol. Struct. 1252 (2022) 132090.

[28] K. Sayin, M. Rezaeivala, S. Erkan, E. Güney, Determination of structural, spectral, computational and OLED properties of Ex2. 2Box^{2+} Cyclophane and its derivatives: experimental and computational study, J. Mol. Struct. 1253 (2022) 132286.

[29] A. Irfan, S. Muhammad, A.R. Chaudhry, A.G. Al-Sehemi, R. Jin, Tuning of optoelectronic and charge transport properties in star shaped anthracenothiophene-pyrimidine derivatives as multifunctional materials, Optik 149 (2017) 321–331 (Stuttg).

[30] M. Cölle, J. Gmeiner, W. Milius, H. Hillebrecht, W. Brütting, Preparation and characterization of blue-luminescent tris (8-hydroxyquinoline)-aluminum (Alq3), Adv. Funct. Mater. 13 (2) (2003) 108–112.

[31] H. Xin, M. Guang, F.Y. Li, Z.Q. Bian, C.H. Huang, K. Ibrahim, F.Q. Liu, Photoluminescence and electroluminescence of the exciplex formed between a terbium ternary complex and N, N′-diphenyl-N, N′-bis (3-methylphenyl)-1, 1′-diphenyl-4, 4′-diamine, Phys. Chem. Chem. Phys. 4 (23) (2002) 5895–5898.

[32] S. Erkan, Structural, spectroscopic and anti-cancer properties of hydroxy-and sulfonamide-azobenzene platinum (II) complexes: DFT and molecular docking studies, Cumhur. Sci. J. 39 (4) (2018) 1036–1051.